



Effects of Mobile Space-Charge on Dynamic Characteristics and Parasitic Resistance of InP Terahertz IMPATT Oscillator Operating at Elevated Junction Temperature

¹Moumita Mukherjee, ²Pravash Tripathi and ³S. P. Pati

¹Centre of MM-Wave Semiconductor Devices and Systems,
Institute of Radio Physics and Electronics, University of Calcutta, India
1, Girish Vidyaratna Lane, Kolkata 700009, West Bengal, India.

²PIET, Rourkela, Odisha

³AICTE Emeritus Professor, NIST, Pelur Hills, Berhampur, Odisha

Abstract

Extensive simulation studies have been carried out for the first time on the feasibility of THz power generation from an InP based Double Drift Transit Time diode operating at elevated junction temperature (250°C). The effects of mobile-space-charge on the THz-frequency performance as well as on the parasitic series resistance (R_S) of the device are also investigated by a generalized simulation scheme. The study reveals that at the optimized bias current density of $3.2 \times 10^8 \text{ Am}^{-2}$, the device is capable of delivering output power density of $3 \times 10^9 \text{ Wm}^{-2}$ with an efficiency of 7%. With the increasing bias current density the space charge effects are found to become prominent and this cause serious degradation of THz performances of the device as far as output power density, efficiency and negative resistivity are concerned. It is observed that at a high bias current density of $7 \times 10^8 \text{ Am}^{-2}$, space charge increases the value of R_S significantly (~38%). These optimized simulation data may be suitably used for fabrication of InP –IMPATT device at 0.3 THz region for application in high-power THz module.

Keywords: Double drift IMPATT, Elevated junction temperature, High power source, Mobile space charge, Parasitic series resistance, Terahertz solid-state source, Transit Time device.

INTRODUCTION

TERAHERTZ (THz) waves, occupying a large portion of the electromagnetic spectrum (300 GHz to 10,000 GHz) between the Millimeter-wave and infrared bands, is the next frontier in basic natural science, medicine and especially in technology. The so called “Terahertz-gap” implies that a big challenge still occurs for Terahertz technology since it is in the margin of electronics and photonics technologies. The region is rich with immense application possibilities

those includes detection of explosives, radio astronomy, space research, earth and ozone-hole monitoring and medicine. However, a major obstacle to the exploitation of the potential is the lack of efficient powerful sources that are also reliable, compact as well as cheap. Systems for rapidly emerging applications at THz frequencies thus require reliable high-power sources. In the last few years [1], the development of suitable sources for this frequency regime is being extensively explored worldwide.

It is already established that **IMPact Avalanche Transit Time (IMPATT)** diodes are the most powerful solid-state sources at MM wave frequencies and are widely used in various civilian and space communication systems as well as in high power radars, missile-seekers etc. *Mukherjee et al.* [2] have recently predicted the prospects of Wide band gap semiconductor based IMPATTs as reliable THz power source. In addition to wide band gap semiconductors, published literatures on InP based IMPATT diodes have also clearly established their superiority over Si IMPATTs in terms of RF power and conversion efficiency [3] at higher MM-wave frequencies. In spite of that the potential of InP as a base material for developing THz IMPATT oscillator at higher junction temperature has not yet been explored. This prompted to authors to study the possibility of generating THz power from a double drift region (DDR, $p^{++} p n n^{++}$ type) InP IMPATT diodes at elevated junction temperature. Junction temperature of IMPATT diodes at THz frequencies under operating condition may increase due to high bias current density and low conversion efficiency of the device. With a proper heat sink arrangement and circular ring geometries, the junction temperature in InP device can be limited to 500K [4]. The purpose of the present research is to carry out realistic analyses of the THz properties of DDR InP IMPATTs by taking the junction temperature as high as 500K.

At high bias current density, mobile space charge in the depletion region of the device plays an important role in degrading the high-frequency characteristics of the diodes. It is thus very important to optimize the bias current density in order to achieve optimum performance from the designed diodes. Thus to get an idea of mobile-space-charge effect, the authors have made a systematic analysis of InP IMPATT diodes operating at wide range of bias current densities.

Parasitic positive series resistance (R_S) is a crucial parameter that characterizes the serious power loss in the substrates and in the metallic contact layers and therefore restricts the output power density. The exact series resistance is difficult to define as it can vary with the chip mounting conditions. However, from the device point of view R_S consists of the summation of substrate resistance, un-depleted epitaxial layer resistance and contact resistances. The doping level and thickness of the epitaxial layer are so chosen that the depletion layer edge at breakdown sweeps almost to the epitaxial layer-substrate interface. This is required to ensure that the parasitic resistance contributed by any high-resistivity epilayer is small. The presence of mobile space charge at high bias current density distorted the device electric field profile, and this may affect the values of R_S also. Thus it is important to study the effects of mobile space charge on the R_S values of THz IMPATT operating at high bias current density.

To the best of authors' knowledge this is the first report on the studies of mobile space charge effects on the high-frequency behavior and parasitic series resistance of THz IMPATTs operating at elevated junction temperature.

1. Simulation Methodology

InP DDR diodes are first designed and optimized through a double iterative simulation technique used for analysis of IMPATT diode [5] in which the effect of space charge is incorporated. The experimental values of material parameters, i.e., temperature and field dependence of carrier ionization rates, drift velocities and high field mobility of charge carriers in InP at 500K [6] are taken as input parameters in the analysis. In order to study the space charge effects, the device is designed to operate within a wide range of bias current density from $1.5 \times 10^8 \text{ Am}^{-2}$ to $7.0 \times 10^8 \text{ Am}^{-2}$, while the device dimension and doping profile are fixed at an optimum value corresponding to a lower punch through effect.

2.1 DC-Analysis

The DC-method, described in details elsewhere [5], considers a generalized ($n^{++} \text{ n p } p^{++}$) structure. Here, n^{++} and p^{++} are highly doped substrates and n and p are epilayers. Summarily, in the DC-method, the computation starts from the field maximum near the metallurgical junction. The distribution of DC electric field and carrier currents in the depletion layer are obtained by a double-iterative simulation method, which involves iteration over the magnitude of field maximum (E_m), and its location in the depletion layer. The method is used for a simultaneous solution of Poisson and carrier continuity equations at each point in the depletion layer. The field boundary conditions are given by,

$$E(-x_1) = 0 \text{ and } E(+x_2) = 0 \quad (1)$$

Here $-x_1$ and x_2 represent the edges of the depletion layer in n and p regions, respectively. The boundary conditions for normalized current density $P(x)$, are given by,

$$P(-x_1) = (2/M_p - 1) \text{ and } P(x_2) = (1 - 2/M_n) \quad (2)$$

$M_n = J/J_{ns}$, $M_p = J/J_{ps}$ where J_{ns} and J_{ps} are electron and hole leakage current densities, respectively. M_p and M_n are hole and electron current multiplication factors, respectively. $P = (J_p - J_n)/J$, where J_p = hole current density, J_n = electron current density and J = total current density.

Thus the DC-field and carrier current profiles are obtained by solving Poisson and carrier continuity equations, when boundary conditions (1) and (2) are satisfied. The realistic field dependence of electron and hole ionization rates, carrier mobility, and the saturated drift velocities of electron ($v_{s,n}$) and hole ($v_{s,p}$) [6] are used in the computation for the profiles of electric field and carrier currents. Background doping concentration (both for n and p-sides) are taken as $4.5 \times 10^{23} \text{ m}^{-3}$, n-epilayer width = 96.5 nm and p-epilayer width = 99 nm. The outputs of DC analysis are then used in the small-signal analysis, described briefly in the next sub-section.

2.2 Small-Signal Analysis

The small-signal analysis of the IMPATT diode provides insight into the high-frequency performance of the diode. The range of frequencies exhibiting negative conductance of the diode can easily be computed by Gummel-Blue method [7]. From the DC-field and current profiles, the spatially dependent ionization rates that appear in the Gummel-Blue equations are evaluated, and

fed as input data for the small-signal analysis. The edges of the depletion layer of the diode, which are fixed by the dc analysis, are taken as the starting and end points for the small-signal analysis. On splitting the diode impedance $Z(x, \omega)$ obtained from Gummel–Blue method, into its real part $R(x, \omega)$ and imaginary part $X(x, \omega)$, two differential equations are framed [8]. A double-iterative simulation scheme incorporating modified Runge-Kutta method is used to solve these two equations simultaneously. The small-signal integrated parameters like negative conductance ($-G$), susceptance (B), impedance (Z), frequency band width, and the quality factor (Q) of the diode are obtained satisfying the boundary conditions derived elsewhere [8]. The analysis provides the high-frequency negative resistance and negative reactance profiles in the space-charge layer of the device. The diode negative resistance ($-Z_R$) and reactance ($-Z_X$) are computed through numerical integration of the $-R(x)$ and $-X(x)$ profiles over the active space-charge layer.

$$\text{Thus, } -Z_R = \int_{-x_2}^{x_1} -R \, dx \quad \text{and, } -Z_X = \int_{-x_2}^{x_1} -X \, dx$$

$$\text{The diode impedance } Z \text{ is given by, } Z(\omega) = \int_{-x_2}^{x_1} -Z(x, \omega) \, dx = -Z_R + jZ_X \quad (3)$$

The diode admittance is expressed as,

$$Y = 1/Z = -G + jB = 1/(-Z_R + jZ_X) \\ \text{or, } -G = -Z_R / ((Z_R)^2 + (Z_X)^2) \quad \text{and} \quad B = Z_X / ((Z_R)^2 + (Z_X)^2) \quad (4)$$

It may be noted that both $-G$ and B are normalized to the area of the diode.

The avalanche frequency (f_a) is the frequency at which the imaginary part, Susceptance (B) of the admittance changes its nature from inductive to capacitive. Again, it is the minimum frequency at which the real part, conductance (G) of the admittance becomes negative. At the avalanche frequency oscillation starts to build up in the circuit.

The small signal quality factor (Q) is defined as the ratio of the imaginary part of the admittance to the real part of the admittance (at the peak frequency), i.e., $-Q_p = (B_p / -G_p)$

At a given bias current density, the peak frequency (f_p) is the frequency at which the negative conductance of the diode is a maximum, and the quality factor is a minimum. At resonance, the maximum RF power output (P_{\max}) from the device is obtained from the expression:

$$P_{\text{RF}} = (V_{\text{RF}}^2 \cdot G_p \cdot A) / 2, \quad (5)$$

where V_{RF} (amplitude of the RF swing) is taken as $V_B/2$, assuming a 50% modulation of the breakdown voltage V_B and A is the area of the diode. The diode negative conductance at the optimum frequency ($-G_p$) is normalized to the area of the diode. The role of parasitic positive series resistance is also considered for calculating realistic values of P_{\max} . The space step for the present simulation is set as 1.0 nm. The validity of this simulation method in THz frequency regime was verified and reported earlier [2] [8].

Adlerstein *et al.* (1983) determined analytically the values of R_S of a DDR IMPATT diode with symmetrical device structure and for equal ionization rates and drift velocities of charge carriers from the measurement of oscillation threshold frequency [9]. Mukherjee *et al.* (2007) [8] have estimated the values of R_S for THz devices under small-signal approximation following the approach of Gummel-Blue and Adlerstein *et al.* [7] [9]. The method used for semi-quantitative estimation of R_S is as follows: The steady state condition for device oscillation is given by [10]:

$$g(\omega) = -G(\omega) - \{B(\omega)\}^2 R_S(\omega) \quad (6)$$

where, g is load conductance. $-G$, B , g are normalized to the area of the diode. The relation provides minimum uncertainty in g at low power oscillation threshold. Under the small-signal condition, R_S can be estimated by considering the value of g nearly equal to the diode conductance (G_D) at resonance.

RESULTS AND DISCUSSION

The DC and high-frequency properties of the device have been studied for different values of bias current densities (J_0) and the results are shown in Table I. The electric field profiles $E(x)$ of the diode at 500K and at different operating current densities are shown in Figure 1. The Figure shows that the peak electric field (E_m) near the metallurgical junction remains almost constant at $8.3 \times 10^7 \text{ Vm}^{-1}$ up to bias current density of $3.2 \times 10^8 \text{ Am}^{-2}$, but the value of E_m decreases on further increase of bias current density. Increase of J_0 from $3.2 \times 10^8 \text{ Am}^{-2}$ to $7 \times 10^8 \text{ Am}^{-2}$ causes E_m to decrease by ~18%. This reduction of E_m occurs due to mobile space charge effect at bias current density greater than $3.2 \times 10^8 \text{ Am}^{-2}$. The Figure also depicts that the field profiles of the diode get distorted and remain high over a wider portion of the depletion layer at higher current densities. This in turn increases the voltage across avalanche region and leads to sharp deterioration of η , because of the decrease of drift voltage (V_D). The similar trend is reflected in the values of η , as shown in Table I. It is observed that the increase of J_0 from $1.5 \times 10^8 \text{ Am}^{-2}$ to $3.2 \times 10^8 \text{ Am}^{-2}$, improves the conversion efficiency from 4.7% to 7%. However, the further increase of J_0 decreases η by 20% of optimum value. Diode breakdown voltage (V_B) is also found to increase initially, up to an operating current density of $3.2 \times 10^8 \text{ Am}^{-2}$. On further increasing J_0 to $5.5 \times 10^8 \text{ Am}^{-2}$, V_B is found to decrease slightly (4%). The variations of η and V_B for different operating current densities are shown in Fig. 2. Figure 2 also shows that the values of V_B and η initially increase with increasing current densities; attain maximum value and then decrease. It is very interesting to observe that as the value of J_0 is increased from $5.5 \times 10^8 \text{ Am}^{-2}$ to $7 \times 10^8 \text{ Am}^{-2}$, V_B increase slightly. This slight increase of V_B at higher current density ($> 5.5 \times 10^8 \text{ Am}^{-2}$) is due to the pronounced mobile space charge effect on electric profile.

Table I: DC and small-signal properties of InP terahertz impatt at 500K.

DC and high-frequency properties	Current density (J_0) (10^8 Am^{-2})			
	1.5	3.2	5.5	7.0
Field Maximum (E_m) (10^7 Vm^{-1})	8.3	8.5	7.5	7.0
Breakdown Voltage (V_B) (V)	9.0	10.8	10.4	10.6
Efficiency (%) $\eta = (V_B - V_a)/(V_B \cdot \pi)$	4.7	7.0	5.8	5.5
Avalanche frequency (f_a) (THz)	0.17	0.17	0.15	0.17
Peak frequency (f_p) (THz)	0.28	0.31	0.35	0.38
Peak Conductance ($-G_p$) (10^6 S m^{-2})	150.0	206.0	247.0	240.0
P_{\max} (Area: 10^9 Wm^{-2})	1.5	3.0	3.4	3.3

The admittance plots of the device for different values of J_0 are shown in Figure 3. It is found that the increase of J_0 from $3.2 \times 10^8 \text{ Am}^{-2}$ to $5.5 \times 10^8 \text{ Am}^{-2}$ increase device negative conductance from $150 \times 10^6 \text{ Sm}^{-2}$ to $247.0 \times 10^6 \text{ Sm}^{-2}$. Further increase of J_0 decrease $-G_p$, as depicted from Fig. 3. This decrease of G_p is due to the effect of pronounced mobile space charge at a current density as high as $7 \times 10^8 \text{ Am}^{-2}$. With the increasing J_0 , peak operating frequency is found to increase. However the peak operating frequency is found to be close with the design frequency (0.3 THz) for the current density of $3.2 \times 10^8 \text{ Am}^{-2}$.

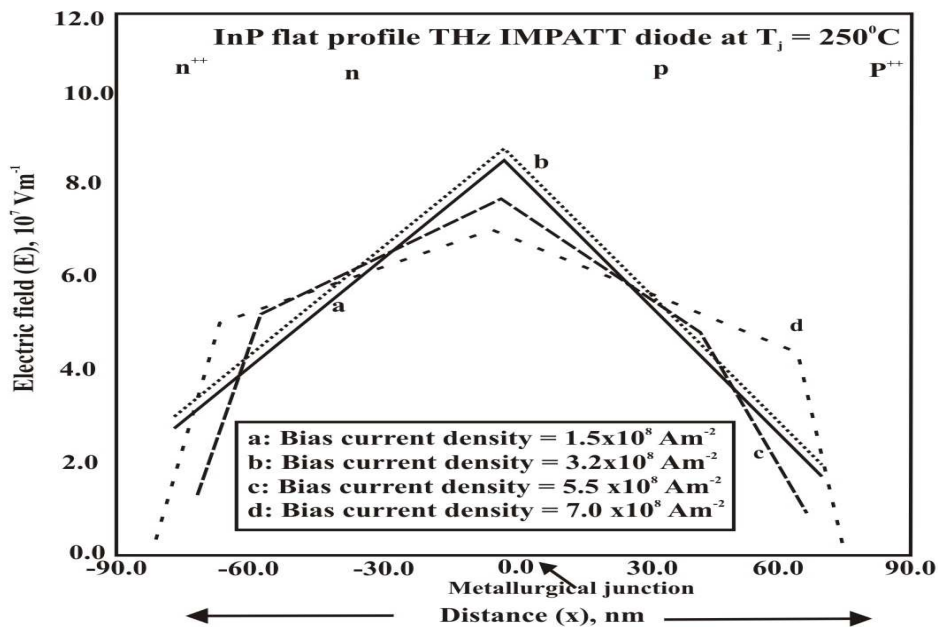


Figure 1. Effects of space charge on electric field profiles $E(x)$ of InP DDR IMPATT diodes at elevated junction temperature

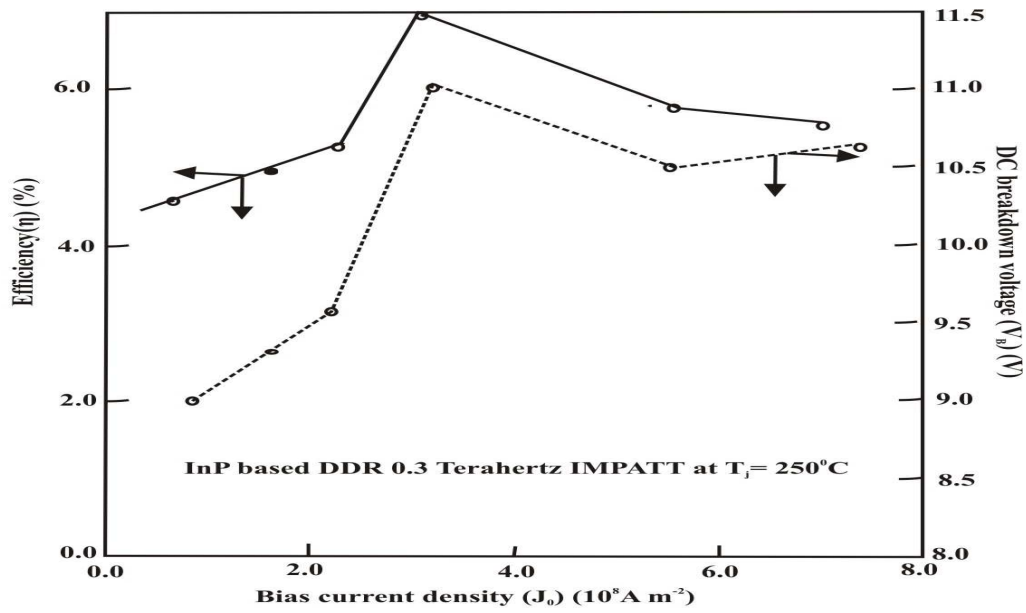


Figure 2. Effects of mobile space charge on Dc to RF conversion efficiency and breakdown voltage of the InP based 0.3 Terahertz IMPATT diode

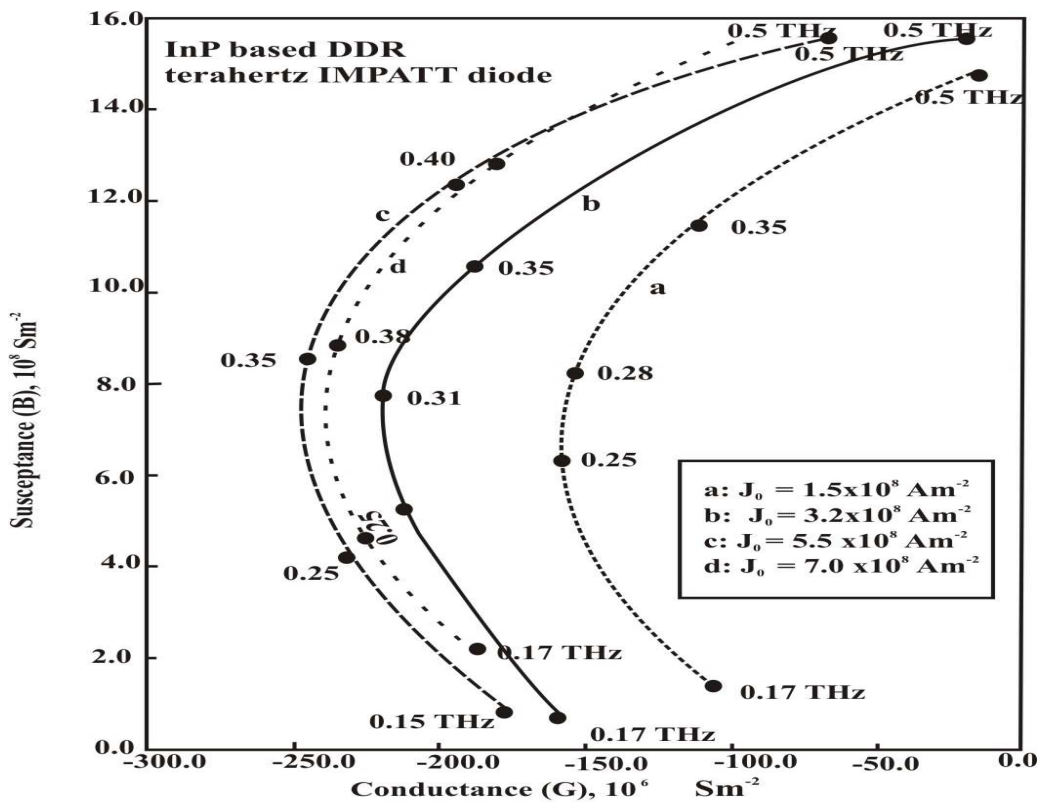


Figure 3. Effects of mobile space charge on admittance plots of InP flat profile DDR IMPATT diodes at terahertz region.

Figure 4 show the negative resistivity $R(x)$ profiles of the THz diode at different current densities. Negative resistivity profiles give a physical insight into the region of the depletion layer that contributes to RF power. The profiles are characterized by two negative resistivity peaks in the middle of the two drift layers of the DDR devices interspaced by a dip located in the avalanche region near the metallurgical junction. It is observed from the Figures that the magnitudes of negative resistivity peaks in the electron and hole drift layers increase slightly up to a current density of $3.2 \times 10^8 \text{ Am}^{-2}$ and thereafter gradually depressed as J_0 is increased further. These decrease of peak magnitudes in $R(x)$ profiles are due to mobile space charge effect. Further, it is found that the negative resistivity peak is much larger in magnitude in hole drift layer than that in electron drift layer for all cases. This phenomenon can be co-related in terms of higher ionization rates of holes in comparison to those of electrons for the entire field range in InP [3].

The effects of mobile space charge on the values of R_S are further studied and the results are shown in Table II. The corresponding values of diode conductance, negative resistance and estimated load conductance are also shown in the same table. The series resistance, R_S , baring the contribution of ohmic contact resistance is estimated from equation (6). For the realistic estimation of R_S , the p-type and n-type contact resistances are also taken into account in the determination of diode total parasitic series resistance, $R_{S, \text{total}}$. A p-type contact resistance $\sim 10^{-6} \Omega \text{ cm}^2$ [10] and n-type contact resistance $\sim 10^{-7} \Omega \text{ cm}^2$ [11] is considered in the analysis of $R_{S, \text{total}}$. It is found from Table II that the increase of J_0 from $1.5 \times 10^8 \text{ Am}^{-2}$ to $3.2 \times 10^8 \text{ Am}^{-2}$ decrease $R_{S, \text{total}}$ slightly by 4%. Further increase of J_0 increase $R_{S, \text{total}}$ significantly (by $\sim 38\%$). Thus the pronounced mobile space charge at a bias current density of $7 \times 10^8 \text{ A m}^{-2}$ seriously affects the values of $R_{S, \text{total}}$. A similar trend is observed in Figure 5, where the effects of mobile space charge on the $R_{S, \text{total}}$ are shown.

Table II: The effects of mobile space charge on $R_{S, \text{total}}$ of InP impatt diodes at 500K (values are estimated at 0.3 THz).

Current density (10^8 Am^{-2})	-ve conductance (-G) (10^6 Sm^{-2})	Susceptance (B) (10^6 Sm^{-2})	Estimated load conductance (g) (10^6 Sm^{-2})	Diode -ve resistance ($-Z_R$) ($10^{-10} \Omega \text{ m}^2$)	Series Resistance ($R_{S, \text{total}}$) ($10^{-10} \Omega \text{ m}^2$)
1.5	130.0	850.0	112.0	1.8	1.4
3.2	192.0	775.0	178.5	3.0	1.3
5.5	230.0	795.0	208.0	3.3	1.6
7.0	240.0	800.0	195.0	3.4	1.8

The above study thus reflects that the optimized bias current density corresponding to highest efficiency, highest breakdown voltage and lowest parasitic series resistance for THz InP IMPATT diode is $3.2 \times 10^8 \text{ Am}^{-2}$. Device negative conductance at this current density is found to be $206.0 \times 10^6 \text{ Sm}^{-2}$ and this further increase to $247.0 \times 10^6 \text{ Sm}^{-2}$ with the increase of current density to $5.5 \times 10^8 \text{ Am}^{-2}$, while the output power density level remains almost constant at $\sim 3 \times 10^9$

Wm^{-2} with the similar increase of bias current density. The study also establishes that InP based double drift IMPATT has potential to generate THz power density of $\sim 3 \times 10^9 \text{ Wm}^{-2}$ with an efficiency of $\sim 11\%$ at 0.3 THz, even when the device junction temperature is increased to 500K. These studies are thus very encouraging for employing InP as a suitable base semiconducting material for developing reliable compact IMPATT source in the THz regime.

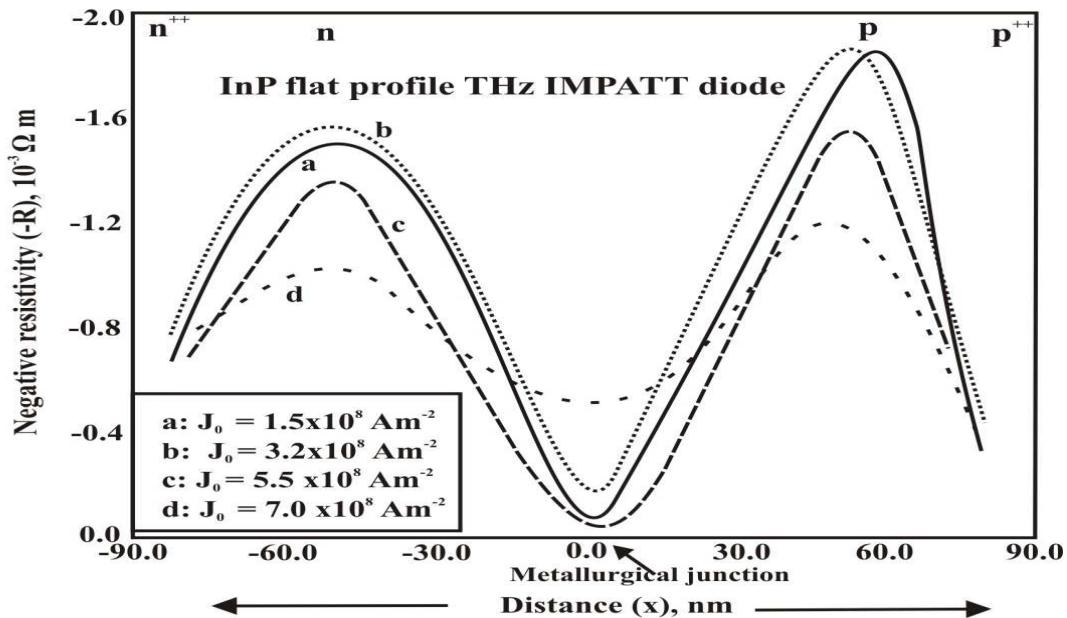


Figure 4. Effect of mobile space charge on negative resistivity profiles of InP Terahertz IMPATT diode at junction temperature = 250°C.

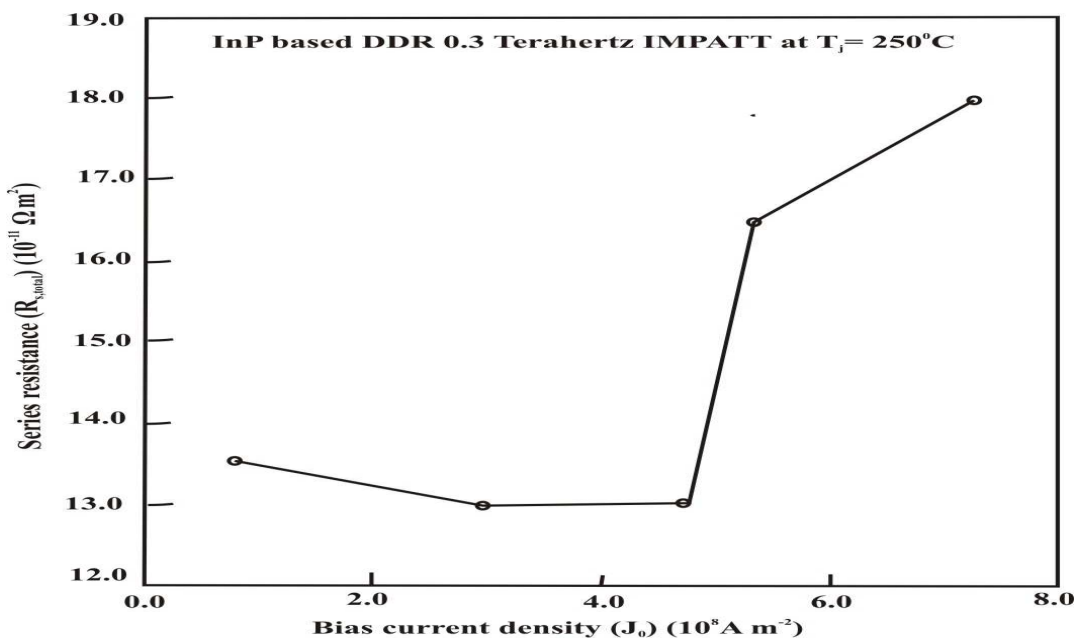


Figure 5. Effects of mobile space charge on series resistance of the InP based 0.3 Terahertz IMPATT diode

CONCLUSION

The simulation studies provide a clear insight into the prospects of InP based DDR IMPATTs as possible THz source. The simulation results, as presented in the paper, on the studies of mobile space charge effects on THz characteristics as well as on the parasitic series resistance will be useful for design optimization of the THz IMPATT diode at elevated junction temperature. Since there are no available experimental results on InP THz IMPATT, no comparison could be made. However, it is proposed that experimental validation of these results might be possible through the following steps:

- 1) To realize the DDR InP IMPATT in reality, a MOCVD based InP (n type substrate, 2-inch) growth sequence is suggested (Figure 6). Undoped InP is to be incorporated to arrest zinc diffusion from p-InP to n-InP. After the growth, the device fabrication follows usual process steps like photo-lithography with appropriate photo mask, mesa formation by reactive ion-etching and deposition of metal contacts. Ti/Pd/Au combination is used as contact materials for p-electrode. Before the deposition of n-metal contact, the substrate is made thin by lapping and polishing. The purpose of thinning is to remove heat (if any generated at junction) immediately. After polishing, AuGe/Au is used as contact materials for n-electrode. (2) Characterization of THz properties might be possible with the device embedded in a corrugated THz wave guide [2]. (3) Measurements of THz power and frequency might be done with a THz VNA (Vector Network Analyser). THz transmission and measurement systems are discussed in earlier research papers [2].

The present results may be used for practical realization of the InP diodes at THz regime for application in interstellar explorers.

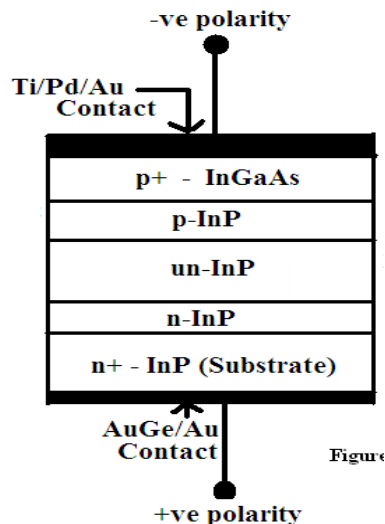


Figure 6. A proposed InP IMPATT growth sequence for operation in the Terahertz frequency region

Acknowledgement

Moumita Mukherjee wishes to acknowledge Defence Research and Development Organisation (DRDO, Ministry of Defence, Govt. of India) and University Grant Commission (UGC, Govt. of India) for awarding her “Senior Research Fellowship” to carry out this work. Prof Pati wishes to express his sincere thanks to AICTE, New Delhi for grant of Emeritus Fellowship in his favour.

REFERENCES

- [1] P. H. Siegel, *IEEE Trans. Microwave Theory Tech.*, **2002**, 50, 3, 910–928.
- [2] M. Mukherjee, N. Mazumder and S.K.Roy, *IEEE Trans. Device Materials Reliability*, **2008**, 8, 608-620.
- [3] M. Mukherjee and N. Mazumder, *Proc. of IEEE-MEET 2007*, Croatia, May 2007, 72-77.
- [4] R. Mukherjee and J. P. Banerjee, *Int. J. Electronics*, **1994**, 76, 4, 589- 600.
- [5] S. K. Roy, J.P. Banerjee and S. P. Pati *Proc.4th Conf. on Num.Anal. of Semiconductor Devices (NASECODE IV) (Dublin)* (Dublin: Boole), **1985**, 494.
- [6] R. K. Mains and G. I. Haddad, *Infrared and Millimeter Waves*, vol. 10, Book chapter- 3, pp. 124-125, **1983**.
- [7] H. K. Gummel and J. L. Blue, *IEEE Trans. Electron Devices*, **1967**, ED –14, 569-580.
- [8] M. Mukherjee *et al*, *Semicond. Sc. & Tech.*, **2007**, 22, 1258.
- [9] M. G. Adlerstein, L. H. Holway, and S. L. Chu, *IEEE Transactions on Electron Devices*, **1983**, ED-30, 179-182.
- [10] M. H. Park, L. C. Wang J. Y. Cheng, C. J. Palmstrom, *Applied Physics Letters*, **1997**, 70, 99-101.
- [11] M.T. Fresina, S.L. Jackson, G. E. Stillman, *Electronics Letters*, **1994**, 30, 2177-2178.